

Doping in the two-dimensional limit: p/n -type defects in monolayer ZnODong Han^{1,*}, Xian-Bin Li^{2,†}, Dan Wang³, Nian-Ke Chen², and Xi-Wu Fan⁴¹*Changchun Institute of Optics Fine Mechanics and Physics, Chinese Academy of Sciences, Changchun 130033, People's Republic of China*²*State Key Laboratory of Integrated Optoelectronics, College of Electronic Science and Engineering, Jilin University, 130012 Changchun, People's Republic of China*³*Department of Mechanical Engineering and Materials Science, Yale University, New Haven, Connecticut 06511, USA*⁴*State Key Laboratory of Luminescence and Applications, Changchun Institute of Optics Fine Mechanics and Physics, Chinese Academy of Sciences, Changchun 130033, People's Republic of China*

(Received 2 June 2021; revised 10 December 2021; accepted 14 December 2021; published 10 January 2022)

The thickness limit is utilized to investigate the doping physics in ZnO, i.e., monolayer (ML) ZnO. First-principles study demonstrates that the p/n -type defects in ML ZnO still have doping asymmetry. Among the doping defect models widely studied in bulk ZnO, Li_{Zn} and Ga_{Zn} with ionization energies of 0.86 and 0.82 eV are the optimal p - and n -type doping defects in ML ZnO, respectively. Their ionization energies are comparable with those of relatively shallow defects in other ML semiconductors. However, the Li_{Zn} acceptor faces a severe issue in that Li_{Zn} is the metastable structure and will transform into the most stable Jahn-Teller-distorted structure ($\text{Li}_{\text{Zn}}^{\text{JT}}$) with increasing its ionization energy to 1.53 eV. Furthermore, our scanning tunneling microscopy simulations show even a little structural distortion of the doping defects can be easily detected with the appropriate positive bias voltage on a sample of ML ZnO. The present study reveals the p/n -type defects' properties in ML ZnO and offers a way to understand and directly identify defect behaviors in wide-band-gap semiconductors in their two-dimensional limit form.

DOI: [10.1103/PhysRevB.105.024104](https://doi.org/10.1103/PhysRevB.105.024104)**I. INTRODUCTION**

Zinc oxide (ZnO) is a typical wide-band-gap semiconductor, whose ultraviolet optoelectronic devices have demonstrated extraordinary performance for decades [1–3], but it is still far from large-scale commercial applications, due to the difficulty of realizing the reproducible and low-resistivity p -type ZnO [4]. For p -type doping in ZnO, the single-chemical-species doping is limited, where the dopants cannot offer sufficient hole concentration because of the low solubility, the large ionization energy, or both [5]. To further ameliorate the doping properties, other doping methods with multiple chemical species, such as codoping [6,7], defect-complex doping [8,9], and molecular doping [10,11], are theoretically proposed. Even though these doping methods are massively performed in experiments [12–16], the microscopic origin behind the p -type ZnO is still unclear. The key reason causing this situation is that the proposed defects are complicated and inside the material, which are hard to create and validate directly on the atomic scale. In other words, these doping methods do little to realize p -type ZnO and comprehending the microscopic mechanism, resulting in not solving the problem of doping asymmetry in this wide-band-gap semiconductor. In fact, a similar complexity of defect physics also exists in other wide-band-gap semiconductors, which seriously hinders the applications, like in ultraviolet optoelectronics.

In recent years, two-dimensional (2D) semiconductors have been extensively developed. For example, 2D ZnO has been theoretically studied [17–19] and successfully synthesized in experiments [19–22]. The outstanding optoelectronic properties of ZnO are not only preserved but also intensified when bulk ZnO is reduced to the atomic thickness. The band gap of bulk ZnO enlarges from 3.37 eV to larger than 4.0 eV [19–21] with the direct-band-gap character [18] for a monolayer (ML). The exciton binding energy of 60 meV of bulk ZnO is expected to be further enhanced, which is universally found in 2D semiconductors [23]. More importantly, in 2D semiconductors, the thickness becomes a naturally controllable dimension that can refine the doping properties, and it provides an opportunity to reexamine the microscopic origin of the doping asymmetry and pursue both p - and n -type doping in wide-band-gap semiconductors.

In this work, we investigate the doping physics in ML ZnO by first-principles calculations and the recently proposed Wang-Li-Zhang method to overcome the energy divergence of charged defects in 2D materials [24,25]. The typical p/n -type defects or defect complex in ZnO were analyzed in the 2D limit. The p/n -type defects in ML ZnO still exhibit doping asymmetry. Among the five acceptor models proposed here (Li_{Zn} , Ag_{Zn} , N_{O} , V_{Zn} , and $\text{N}_{\text{O}}\text{-V}_{\text{Zn}}$), Li_{Zn} with the formation energy (ΔH_f^0) of 2.57 eV has the smallest ionization energy (IE) of 0.86 eV, close to that of the shallow donors in ML ZnO and comparable to the relatively shallow acceptors and/or donors in other popular ML semiconductors. However, Li_{Zn} occurs the Jahn-Teller distortion ($\text{Li}_{\text{Zn}}^{\text{JT}}$), which lowers the ΔH_f^0 by 0.68 eV but increases its IE to 1.53 eV. For donor models (Al_{Zn} , Ga_{Zn} , and In_{Zn}), Ga_{Zn} with ΔH_f^0 of 1.69 eV

*hand@ciomp.ac.cn

†lixianbin@jlu.edu.cn

and IE of 0.82 eV is the superior candidate for n -type doping. Furthermore, by way of engineering the Coulomb screening environment around 2D ZnO, most acceptors' IEs can be further reduced by ≈ 0.9 eV while the donors' IEs can be reduced by ≈ 0.3 eV according to the binding energies from defect-bound band-edge states. Finally, we demonstrated that these doping defects can be distinctly identified by the surface characterization techniques, such as scanning tunneling microscopy (STM), even if a little structural distortion happens. Our present results propose the possible p/n -type doping candidates in ML ZnO, which should be worth further study in experiments and also offers an alternative strategy to understand and identify the defect behaviors in wide-band-gap semiconductors through their 2D limit form.

II. COMPUTATIONAL METHODS

A. Geometry optimization, total-energy calculation, and STM simulation

Our calculations were performed using density functional theory (DFT) [26,27], as implemented in the VASP codes [28,29]. Projector augmented-wave potentials were used to describe the core electrons, and the cutoff energy for the plane-wave basis was set to 540 eV. To balance the adequate calculation accuracy against the finite computational resources, we employed the Perdew-Burke-Ernzerhof (PBE) functional [30] for geometry optimization and Heyd-Scuseria-Ernzerhof (HSE06) functional [31,32] for total-energy calculation. During the geometry optimization, all atoms could relax until the Hellman-Feynman forces on individual atoms were less than 0.03 eV/Å. In HSE06 calculations, 37.5% of screened Hartree-Fock exchange was mixed to the PBE exchange functional and the screening parameter was set to 0.2 Å⁻¹. According to the present setup, the calculated lattice constant $a = b = 3.289$ Å, $c/a = 1.614$, of bulk ZnO is only 1.2%, 0.8% larger than the experimental value [33], and the calculated band gap of 3.28 eV of bulk ZnO is very close to the experimental measurement [34]. For ML ZnO constrained in the c direction, the supercell approach was induced to model the defects. The supercell varies from 6×6 (72 atoms) to 8×8 (128 atoms) unit cells for $L_a \times L_b$ with the vacuum of 20 Å for L_c . The Monkhorst-Pack k -point mesh grids are $2 \times 2 \times 1$ for geometry optimization and Γ point for total-energy calculation, respectively. In the case of the supercell with Zn-substituted Li, the optimized geometry and total-energy calculation are performed in DFT calculation with both PBE and HSE06 functionals. The simulated STM images are obtained from a constant current mode in the Tersoff-Hamann approach [35]. In this approach, the tunneling current is proportional to the local density of states integrated from the selected energy (e.g., the bias voltage on the sample) to the Fermi level.

B. Formation energy, ionization energy, and Coulomb binding energy

The formation energy for a defect d with charge q is defined as [36–38]

$$\Delta H_f^q(d) = E^q(d) - E(\text{host}) + \sum_i n_i (E_i + \mu_i) + q(\varepsilon_{\text{VBM}} + \varepsilon_F), \quad (1)$$

where $E^q(d)$ is the total energy of the supercell containing a defect d with charge q , and $E(\text{host})$ is the total energy of the perfect host supercell. n_i is the number of atoms of element i being exchanged during the defect's formation between the host supercell and the atom reservoir with the energy $E_i + \mu_i$, where E_i is the energy per atom in the stable phase of element i , and μ_i is the chemical potential with respect to E_i . ε_{VBM} is the valance-band maximum (VBM) of the host supercell and ε_F is the Fermi energy with respect to ε_{VBM} . In a semiconductor material, the ε_F typically varies from the VBM to the conduction-band minimum (CBM). Under thermal equilibrium conditions, the chemical potentials of host atoms, μ_i , must satisfy $\mu_{\text{Zn}} + \mu_{\text{O}} = \Delta H(\text{ML ZnO})$, where $\Delta H(\text{ML ZnO})$ is the formation enthalpy of ML ZnO. In our calculation, the $\Delta H(\text{ML ZnO})$ is -2.71 eV. Therefore, the μ_i , reflecting the growth condition, varies from $\mu_{\text{Zn}} = 0$ eV ($\mu_{\text{O}} = -2.71$ eV) for the Zn-rich (O-poor) condition to $\mu_{\text{Zn}} = -2.71$ eV ($\mu_{\text{O}} = 0$ eV) for the O-rich (Zn-poor) condition. The chemical potentials of external atoms, μ_i , are limited by avoiding the formation of a secondary phase during the growth.

The IE of a defect d , which is determined by its transition level, can be written as follows:

$$\text{IE}(d) = \begin{cases} \frac{E^q(d) - E^{q'}(d)}{q' - q} - \varepsilon_{\text{VBM}} & \text{for acceptor} \\ \varepsilon_{\text{CBM}} - \frac{E^q(d) - E^{q'}(d)}{q' - q} + \varepsilon_{\text{VBM}} & \text{for donor,} \end{cases} \quad (2)$$

where $E^q(d)$ [or $E^{q'}(d)$] is the total energy of the supercell containing a defect d with charge q (or q'). For an acceptor (p type) with trapping one electron, the two different charge states are $q = 0$ and $q' = -1$. For a donor (n type) with exciting one electron, the two different charge states are $q = +1$ and $q' = 0$. ε_{VBM} (ε_{CBM}) is the VBM (CBM) of the host supercell.

Note that the IE in the 2D system is size dependent, because of the long-range Coulomb interaction between the charged defect and the compensating jellium charge. Here, we solved this problem by employing the state-of-the-art defect evaluation method in our previous work [24],

$$\text{IE}_0 = \text{IE}(S, L_c) - \frac{\alpha}{\sqrt{S}} - \left(\frac{\beta}{S}\right) L_c, \quad (3)$$

where IE_0 is the true, size-independent ionization energy, and $\text{IE}(S, L_c)$ is the size-dependent ionization energy with respect to S and L_c . S and L_c are the lateral size and vacuum size of the supercell, respectively. α is the defect-specific Madelung constant and $\beta = e^2/24\varepsilon_0$. The IE_0 is obtained by fitting Eq. (3) with supercell models varying from 6×6 to 8×8 unit cells for $L_a \times L_b$ with the vacuum of 20 Å for L_c .

Due to finite computational resources, we used IE_0^{HSE} , instead of IE_0^{HSE} obtained with Eq. (3) from HSE06 calculations, with

$$\text{IE}_0^{\text{HSE}} = \text{IE}^{\text{HSE}}(6 \times 6) + \text{IE}_0^{\text{PBE}} - \text{IE}^{\text{PBE}}(6 \times 6), \quad (4)$$

where $\text{IE}^{\text{HSE}}(6 \times 6)$ [$\text{IE}^{\text{PBE}}(6 \times 6)$] is the size-dependent IE, calculated in HSE06 (PBE) with the specific lateral size (6×6 supercell model). The IE_0^{PBE} is the size-independent IE obtained with Eq. (3) from PBE calculations. Therefore, the size-independent IE_0^{HSE} [the IEs shown in Fig. 3(a)] is

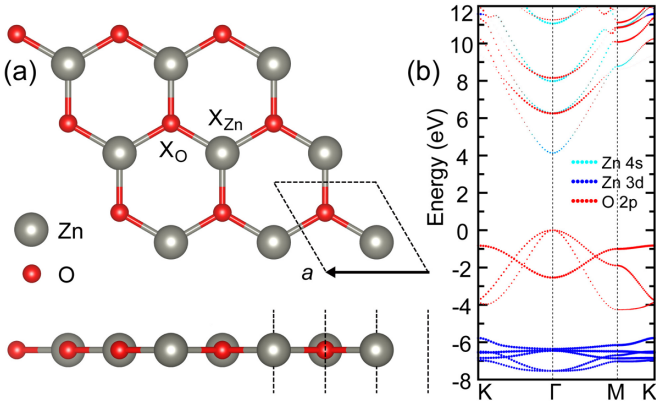


FIG. 1. (a) The atomic geometry of ML ZnO and the impurity X doping. X_{Zn} , X at the Zn site; X_O , X at the O site. (b) The band structure of ML ZnO. The size of dots is proportional to the projection of the electronic wavefunction onto the angular momenta of Zn (cyan, Zn 4s; blue, Zn 3d) or O (red, O 2p).

equal to $IE_0^{HSE}(6 \times 6)$ with adding the correction of $IE_0^{PBE} - IE_0^{HSE}(6 \times 6)$. We have compared the energy difference between IE_0^{HSE} and IE_0^{PBE} of the Li_{Zn} acceptor, as shown in Fig. S1 in the Supplemental Material (SM) [39]. It shows that the energy difference is less than 0.02 eV.

The Coulomb binding energy (E_{db}) between the excited carrier at the defect-bound band-edge (DBBE) state and its corresponding ionized defect is calculated by the fixed occupation method [40], which is performed in the constrained DFT calculation with the HSE06 functional. The defect states for trapping an electron excited from VBM (acceptor) or exciting an electron to CBM (donor) are denoted by arrows in Fig. S2 in the SM [39]. For acceptors, because of the energy convergence issue, the calculated binding energies are coarse. The error of the V_{Zn} -related defects' E_{db} s are smaller than 0.5 eV and the others are no more than 0.1 eV. For donors, to minimize this energy deviation at the Γ point due to the delocalized defects' states in the finite supercell, we used the M point in the Brillouin zone for the ground-state and constrained-DFT calculations. The error of the donors' E_{db} s are smaller than 0.1 eV.

III. RESULTS AND DISCUSSION

A. Atomic and electronic properties of ML ZnO

As shown in Fig. 1(a), the ML ZnO has a graphenelike structure without buckling in the c direction, where Zn and O occupy the two sublattices, respectively. It is generally called graphenelike ZnO (g-ZnO) [41], which is chemically stable from theoretical predictions [18] and experimental verifications [19–21]. Here, the calculated lattice constant a of ML ZnO is 3.289 Å, which is well consistent with the experimental observations [19,42]. This lattice constant is almost the same as that of bulk ZnO. As a result, the bond length of Zn-O in ML is 1.899 Å, about 5.2% shorter than that of 2.004 Å in bulk. Figure 1(b) shows the band structure of ML ZnO. It is found that the ML ZnO still retains the key advantage of direct-band-gap character, and the band gap is greatly larger than that of bulk ZnO. The band gap in our DFT-

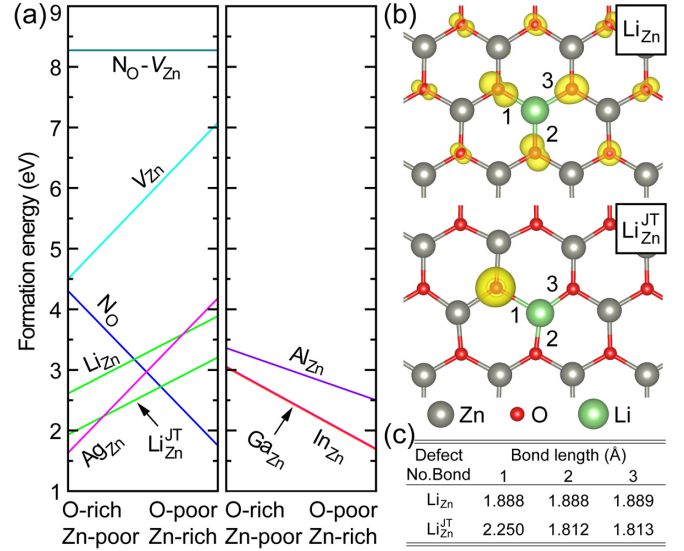


FIG. 2. (a) The formation energy of neutral doping defects in ML ZnO varies along with the growth condition. (b) The optimized atomic geometry of Zn-substituted Li without (Li_{Zn}) and with (Li_{Zn}^{JT}) Jahn-Teller distortion and the corresponding spatial charge density of Li_{Zn} -induced unpaired hole are shown. The corresponding unpaired-hole states are indicated by arrows in Fig. S2 in the Supplemental Material [39]. The isosurface of the charge density distribution is $0.005 e/\text{Å}^3$. (c) The Li-O bond length around the Li impurity in ML ZnO with Li_{Zn} and Li_{Zn}^{JT} defects. The bond number (No. Bond) is labeled in (b).

HSE06 calculation is 4.13 eV, which is in agreement with the experimental measurements of 4.0 eV [20] and 4.48 eV [19]. Moreover, the valence band (VB) mainly consists of O 2p and Zn 3d orbitals, while the conduction band (CB) is mainly contributed by the hybridization of O 2p and Zn 4s orbitals. For the VB, the contributions from the O 2p orbital and Zn 3d orbital are apparently separated, where the O 2p orbital dominantly locates at the energy of 0–4 eV below the VBM, and the Zn 3d orbital dominantly locates at 6–8 eV below the VBM. For CB, the Zn 4s orbital dominates the CBM.

B. Doping defects' atomic configuration and formation energy

In bulk ZnO, various acceptor models including point defects or defect complexes have been explored to quantify its contribution to the p -type conductivity. Here, we take five typical acceptors, e.g., the substituted defects Li_{Zn} [43–45], Ag_{Zn} [46,47], and N_O [43,48], the native defect V_{Zn} [49–51], and the defect complex N_O-V_{Zn} [8], which are popular in bulk ZnO as examples, and investigate their doping properties in ML ZnO. The typical donors, Al_{Zn} , Ga_{Zn} , and In_{Zn} are also studied in ML ZnO as a comparison. The optimized atomic structures and the bond lengths of these defects or defect complex are shown in Fig. S3 and Table S1 in the SM [39]. It is found that most of the substituted defects are on site preserving the lattice symmetry, and the bond length of impurity-O (or -Zn) varies monotonically along with the atomic radius of the doping element. The formation energy (ΔH_f^0) of these neutral defects is shown in Fig. 2(a). The ΔH_f^0 of Ag_{Zn} and N_O vary largely along with the growth condition, only 1.55 and 1.67 eV un-

der their favorable growth conditions, increasing to 4.26 and 4.38 eV under the adverse growth conditions, respectively. For native V_{Zn} , even though its ΔH_f^0 changes a lot along with the growth condition, the lowest ΔH_f^0 of 4.44 eV is still too high, indicating V_{Zn} scarcely forms during the equilibrium growth of ML ZnO. Because of the contradictory growth condition between N_O and V_{Zn} , their complex N_O-V_{Zn} has a remarkably high ΔH_f^0 of 8.27 eV under any growth condition. The high ΔH_f^0 of N_O-V_{Zn} in ML is consistent with that in bulk [8,9], where a special process is necessary to form the N_O-V_{Zn} complex [8].

In previous studies [44,45], the Zn-substituted Li in bulk ZnO was demonstrated to possess two stable atomic configurations: Li at the Zn site (Li_{Zn}) and Li off the Zn site with Jahn-Teller distortion (Li_{Zn}^{JT}). A similar phenomenon is also found in ML ZnO. As shown in Figs. 2(b) and 2(c), all three Li-O bonds in Li_{Zn} have the same bond length of 1.89 Å with preserving the lattice symmetry, while the atomic structure of the Li_{Zn}^{JT} is obviously distorted, where one of the Li-O bonds noticeably elongates to 2.25 Å and the other two Li-O bonds shorten to 1.81 Å. The structural distortion of a defect always accompanies the charge density redistribution of the carrier at the defect state. From the charge density distribution, we can find that the Li_{Zn} -induced unpaired hole delocalizes around the nearby O ions, while the Li_{Zn}^{JT} -induced unpaired hole clearly localizes at the O ion of the elongated Li-O bond. Our DFT-HSE06 calculations show Li_{Zn}^{JT} is more stable than Li_{Zn} in ML ZnO. Li_{Zn} has a relatively low ΔH_f^0 of 2.57 eV under the Zn-poor condition, and the structural distortion can further lower its ΔH_f^0 by 0.68 eV. This energy drop is very close to that of the 0.64 eV we calculated in bulk ZnO. The more stable Li_{Zn}^{JT} indicates that Zn-substituted Li in ML ZnO dominantly exists in the form of the distorted structure. As a comparison, the donor defects have relatively low ΔH_f^0 . The ΔH_f^0 of Al_{Zn} , Ga_{Zn} , and In_{Zn} are 2.50, 1.69, and 1.69 eV under the Zn-rich condition, respectively. Note that these Zn-substituted donors abnormally prefer forming under the Zn-rich condition, rather than the Zn-poor condition, because it avoids the formation of the secondary compounds of group-III oxides. Therefore, according to the ΔH_f^0 , Li_{Zn}^{JT} , Ag_{Zn} , N_O , and those donor defects can form under their favorable growth conditions. In contrast, the V_{Zn} and N_O-V_{Zn} complex hardly form in ML ZnO due to their high formation energies under the equilibrium growth condition.

C. Doping defects' ionization energy

To evaluate the possibility of a defect offering free carriers to the band edge for conductivity, the IE (see the definition in Methods) as well as the corresponding binding energy (E_{db} , see the explanation below) of these defects are shown in Fig. 3(a). In general, both acceptors and donors exhibit relatively deep defect levels, resulting in remarkably large IEs. Compared with those in bulk [47,48], the IEs of N_O and Ag_{Zn} significantly increase to 3.55 and 2.38 eV, respectively, indicating these defects are not active acceptors in ML ZnO. The V_{Zn} , which theoretically predicts the deep acceptor in bulk [50,51], is also an inactive acceptor in ML ZnO because of its IE of 2.65 eV. Besides, the V_{Zn} -related complex fails to generate free holes since the hole states are mainly con-

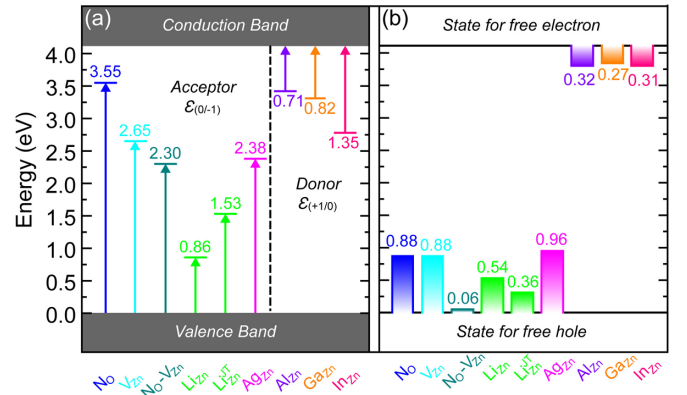


FIG. 3. The ionization energy (IE) and the corresponding binding energy E_{db} of doping defects in ML ZnO. (a) The value close to the colored line is IE, which is the energy of an electron excited from VBM to the transition level $\epsilon_{(0/-1)}$ for acceptors, and the energy of an electron excited from the transition level $\epsilon_{(+1/0)}$ to CBM for donors, respectively. (b) The value close to the color bar is E_{db} , which is the Coulomb energy between the ionized carrier (at DBBE state) and the charged doping defect.

tributed by the V_{Zn} part. In our results, the IE of the N_O-V_{Zn} complex is as large as 2.30 eV. It reveals that the strategy of using V_{Zn} -related complexes as the shallow acceptors in bulk [8,13,52] does not work in ML ZnO. Among the five typical acceptors, the Li-doped defects exhibit the shallowest acceptor levels, but the IEs of two stable Li-doped defects are noticeably different. The metastable Li_{Zn} has the shallowest acceptor level with the IE of only 0.86 eV, while the most stable Li_{Zn}^{JT} pushes its IE to 1.53 eV. Similar results on the Li-doped defects are also found in bulk ZnO. Our calculations show that the metastable Li_{Zn} and most stable Li_{Zn}^{JT} have IEs of 0.18 and 0.86 eV, respectively. As a comparison with these acceptors, the IEs of donors are much smaller. The IEs gradually decrease from 1.35 eV for In_{Zn} , to 0.82 eV for Ga_{Zn} , to 0.71 eV for Al_{Zn} . Generally, due to the weak Coulomb screening in the 2D system, the IE of a defect can separate into two parts: (1) the energy for a carrier excited from the defect state to the DBBE state and (2) the energy (E_{db}) for a carrier to be excited from the DBBE state to the free band-edge state [53]. The latter part, E_{db} , can be reduced by enhancing the Coulomb screening, such as increasing the thickness of the 2D material [25] or introducing a dielectric substrate [54]. As a result, the IE of a defect can be controllably decreased. As shown in Fig. 3(b), the E_{db} s of most acceptors are around 0.9 eV, while the E_{db} s of donors represent energies of around 0.3 eV. It indicates that dielectronic screening engineering can partially reduce the IEs of both acceptors and donors in ML ZnO.

Considering the IEs of the p/n -type defects in ML ZnO, the ML ZnO still has the phenomenon of doping asymmetry. Among the five typical acceptor models, Li_{Zn} has the smallest IE of 0.86 eV, which is close to those of the shallow donors. However, the metastable Li_{Zn} undergoes a Jahn-Teller distortion (Li_{Zn}^{JT}) and increases its IE to 1.53 eV. Besides, according to our molecular dynamics simulation at 800 K as shown in Fig. S4 in the SM [39], the charged Li_{Zn}^+ in ML ZnO is quite

stable, avoiding Li diffusing and forming the donor interstitial defect Li_i . For n -type doping in ML ZnO, Al_{Zn} and Ga_{Zn} have relatively small IEs of 0.71 and 0.82 eV, respectively. But Ga_{Zn} is the superior candidate for n -type doping since the ΔH_f^0 of Ga_{Zn} is much smaller than that of Al_{Zn} .

D. Ionization energies compared to those of other popular ML semiconductor materials

After obtaining the absolute value of the IEs, the concern is whether these defects are shallow (or deep) in ML ZnO. The principle of evaluating the defects in the ML material should be different from that in bulk material since the mechanisms of carrier excitation and transport in ML materials are unique [53,55]. Herein, we compare the defects' IEs in ML ZnO to those of other popular ML semiconductors. The defects' IEs in ML black phosphorus (BP) [25], InSe [56], MoS_2 [53], BN [24], and the present ML ZnO are collected and summarized in Table I. It can be found that the defects' IEs in ML semiconductors are deep generally. The asymmetry between p - and n -type defects' IEs is a general phenomenon in ML semiconductors, where the narrow-band-gap materials hold a stronger asymmetric tendency than the wide-band-gap ones. For example, in ML ZnO, the IEs of the shallowest Li_{Zn} acceptor and Al_{Zn} donor are 0.49 and 0.45 eV, respectively, while in ML BP, the IEs of the shallowest V_P acceptor and Te_P donor are 0.36 and 0.67 eV, respectively.

Note that the band gap of a semiconductor is usually underestimated in DFT-PBE calculations. Here, the higher-level calculations with hybrid functionals (DFT-HSE06) are further performed in ML ZnO to correct the band gap and reevaluate IE. We find that the results of defects' IEs in HSE calculations are mostly like those in PBE calculations, indicating the PBE calculations are reasonable. In ML semiconductors, these doping defects seem to hold the ability to supply the free carriers. For example, doping in MoS_2 has been massively studied in experiments, and Nb doping is verified to be an effective way to grow p -type MoS_2 . The n -type conductivity of as-grown ML MoS_2 is strongly suppressed by Nb doping [57] and the hole carrier concentration in Nb-doped multilayer MoS_2 can also reach 10^{19} – 10^{20} cm^{-3} [58,59]. From this point of view, we can infer that the shallowest acceptor Li_{Zn} is likely a p -type doping defect in ML ZnO, because its IE (0.49 eV in PBE) is close to that (0.55 eV in PBE) of Nb doping in ML MoS_2 . However, the DFT-HSE06 calculations demonstrate that the more stable Li_{Zn}^{JT} with the large IE of 1.52 eV makes Li as a p -type doping impurity face a severe challenge.

E. Simulated STM images for p/n -type defects in ML ZnO

Currently in experiments, it remains a challenge to identify an individual defect directly in bulk ZnO. There is a big gap between the theoretical prediction and the experimental validation. However, taking the thickness advantage of ML ZnO, the defect can be easily detected *in situ* by advanced surface characterization techniques, such as by STM. Herein, the STM images of defects are simulated for guiding the experimental validation in the future. As shown in Fig. 4 and Fig. S5 in the SM [39], it is found that the bright (dark) STM area of perfect ML ZnO is the position of the Zn (O) site

TABLE I. The summary of defects' IEs in various ML materials. The band gap of various ML materials is determined theoretically from the DFT calculations with the corresponding exchange-correlation (XC) functionals.

Host material	Band gap (eV)	IE (eV)		XC functional		
		Acceptors	Donors			
BP ^a	0.91	V_P	0.36	Te_P	0.67	PBE
		P_i	0.48	Se_P	0.69	
				S_P	0.74	
				Op	1.02	
InSe ^b	1.42	Bi_{Se}	0.72	Ge_{In}	0.41	PBE
		V_{In}	0.74	Sn_{In}	0.42	
		Hg_{In}	0.74	Cl_{Se}	0.46	
		Sb_{Se}	0.79	Br_{Se}	0.47	
		Cd_{In}	0.79	I_{Se}	0.51	
		As_{Se}	0.83	Pb_{In}	0.73	
		Zn_{In}	0.84			
		V_{Se}	1.87			
MoS_2 ^c	1.66	Nb_{Mo}	0.55	Re_{Mo}	0.45	PBE
		V_{Mo}	1.04	Mo_S	1.24	
		S_{Mo}	1.22	Mo_{2S}	1.44	
		V_{2S}	1.45			
		V_S	1.55			
BN ^d	4.67	V_B	1.44	C_B	2.03	PBE
		C_N	1.86	V_N	2.50	
ZnO	1.68	Li_{Zn}	0.49	Al_{Zn}	0.45	PBE
		V_{Zn}	1.00	Ga_{Zn}	0.54	
		$N_{O-V_{Zn}}$	1.07	In_{Zn}	0.84	
		Ag_{Zn}	1.14			
		N_O	1.45			
ZnO	4.13	Li_{Zn}	0.86	Al_{Zn}	0.71	HSE06
		Li_{Zn}^{JT}	1.53	Ga_{Zn}	0.82	
		$N_{O-V_{Zn}}$	2.30	In_{Zn}	1.35	
		Ag_{Zn}	2.38			
		V_{Zn}	2.65			
		N_O	3.55			

^aReproduced with permission from Ref. [25].

^bReproduced with permission from Ref. [56].

^cReproduced with permission from Ref. [53].

^dReproduced with permission from Ref. [24].

at the positive bias voltage of $\epsilon_{CBM} - \epsilon_F + 2$ V on the ML ZnO sample, while the O site and surroundings are bright (the dark point at the Zn site) at the negative bias voltage of $\epsilon_F - \epsilon_{VBM} + 1$ V. This observation is in good agreement with the projected band structure of ML ZnO, as shown in Fig. 1(b). In general, the defects are easier to observe in the STM images at the positive bias voltage of $\epsilon_{CBM} - \epsilon_F + 2$ V because the energy dispersion is larger near the CBM in the band structure than that near the VBM. As a result, the defect state is less buried by the bulk states at the same integrated energy range. More importantly, we found that even a little change in the defect's atomic configuration can be easily distinguished in STM images. This is because a little structural distortion of a defect can lead to a significant change in the charge distribution of the defect state. For example, Li_{Zn} forms a hexagonal

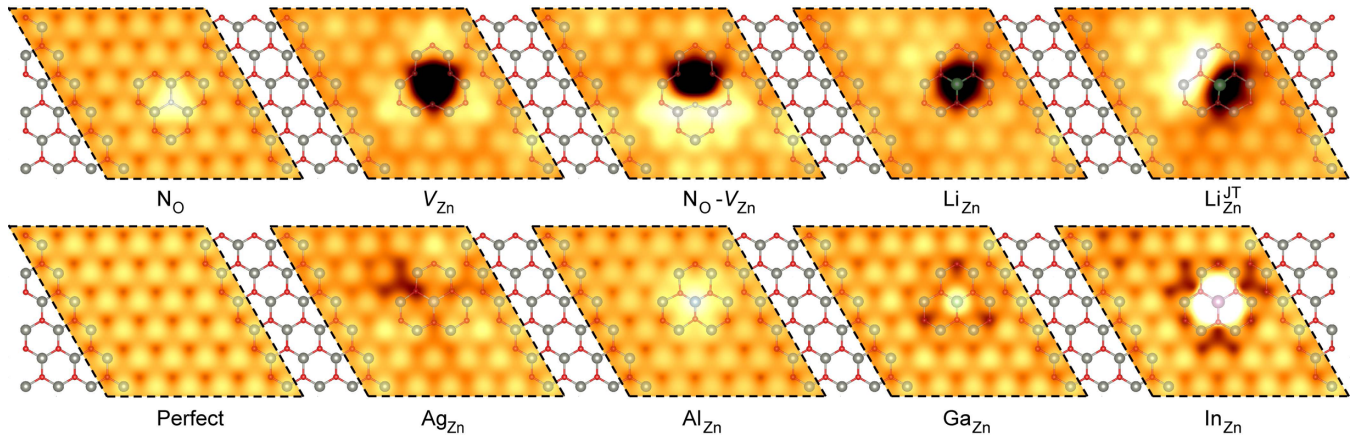


FIG. 4. Simulated STM images of ML ZnO without and with defects in a 6×6 supercell. The charge density is calculated from ε_F to $\varepsilon_{\text{CBM}} + 2$ eV, standing for the positive bias voltage of $\varepsilon_{\text{CBM}} - \varepsilon_F + 2$ V on sample. The corresponding atomic configurations of both ML ZnO and defects are positioned on top of the STM images.

dark area, but the STM image of $\text{Li}_{\text{Zn}}^{\text{JT}}$ is appreciably different. The bright and dark areas are separated by the elongated Li-O bond. Because of the localized unpaired hole distribution on the O of the elongated Li-O bond as shown in Fig. 2(b), the O of the elongated Li-O bond with two bonding Zn ions forms the bright area, while the Li with two other bonding O ions forms the dark area (i.e., shorter Li-O bonds). Similarly, the V_{Zn} and $\text{N}_{\text{O}}-V_{\text{Zn}}$ can also be distinguished in the STM images. Therefore, unlike the challenge of identifying the individual defect in bulk ZnO, our simulated STM images demonstrated that the defect in ML ZnO can be facile to distinguish in the experiment. Recently, STM experiments [60,61] successfully observed the defects near the surface of bulk ZnO, which further ensures the possibility of identifying the defects in ML ZnO. For n -type doping defects in ML ZnO, the unique STM patterns of doping defects also suggest clear identification in experiments.

IV. CONCLUSIONS

In conclusion, our study enlightens an alternative strategy, which utilizes the thickness limit to comprehend the doping properties in wide-band-gap semiconductors. The strategy has one prerequisite, i.e., that the electronic or optoelectronic properties of bulk semiconductors should be basically pre-

served when their bulk form shrinks down to the 2D limit, and one advantage, i.e., that the defects can be easily validated *in situ* by advanced surface characterizations, such as STM. Doping in ML ZnO is such a felicitous example. Here, we found that p/n -type doping defects in ML ZnO still exhibit doping asymmetry. Among the doping defects proposed, Li and Ga are the optimal p/n -type doping impurities with the defects of Li_{Zn} and Ga_{Zn} , respectively. However, the Li_{Zn} is the metastable configuration, while the more stable configuration $\text{Li}_{\text{Zn}}^{\text{JT}}$ with higher IE makes the Li unlikely as an effective p -type doping impurity. Our strategy on studying ZnO doping in its 2D limit could be a way to comprehend the complicated defect physics in traditional wide-band-gap semiconductors for developing their advanced optoelectronic applications.

The authors used the VESTA software package to generate the figures [62].

ACKNOWLEDGMENTS

D.H. would like to thank Yu-Yang Zhang for helpful discussions on STM simulation. Work was supported by the National Natural Science Foundation of China (Grants No. 11974344, No. 61922035, and No. 11874171) and the Open Fund of the State Key Laboratory of Integrated Optoelectronics (Grant No. IOSKL2020KF07).

-
- [1] Z. K. Tang, G. K. L. Wong, P. Yu, M. Kawasaki, A. Ohtomo, H. Koinuma, and Y. Segawa, *Appl. Phys. Lett.* **72**, 3270 (1998).
 - [2] H. Zhu, C.-X. Shan, B. Yao, B.-H. Li, J.-Y. Zhang, Z.-Z. Zhang, D.-X. Zhao, D.-Z. Shen, X.-W. Fan, Y.-M. Lu, and Z.-K. Tang, *Adv. Mater.* **21**, 1613 (2009).
 - [3] A. Tsukazaki, A. Ohtomo, T. Onuma, M. Ohtani, T. Makino, M. Sumiya, K. Ohtani, S. F. Chichibu, S. Fuke, Y. Segawa, H. Ohno, H. Koinuma, and M. Kawasaki, *Nat. Mater.* **4**, 42 (2005).
 - [4] U. Özgür, Y. I. Alivov, C. Liu, A. Teke, M. A. Reshchikov, S. Doğan, V. Avrutin, S. J. Cho, and H. Morkoç, *J. Appl. Phys.* **98**, 041301 (2005).
 - [5] K. Yim, J. Lee, D. Lee, M. Lee, E. Cho, H. S. Lee, H.-H. Nahm, and S. Han, *Sci. Rep.* **7**, 40907 (2017).
 - [6] Y. Yan, J. Li, S.-H. Wei, and M. M. Al-Jassim, *Phys. Rev. Lett.* **98**, 135506 (2007).
 - [7] L. G. Wang and A. Zunger, *Phys. Rev. Lett.* **90**, 256401 (2003).
 - [8] L. Liu, J. Xu, D. Wang, M. Jiang, S. Wang, B. Li, Z. Zhang, D. Zhao, C.-X. Shan, B. Yao, and D. Z. Shen, *Phys. Rev. Lett.* **108**, 215501 (2012).
 - [9] D. Y. Yong, H. Y. He, Z. K. Tang, S.-H. Wei, and B. C. Pan, *Phys. Rev. B* **92**, 235207 (2015).

- [10] J. Bang, Y.-Y. Sun, D. West, B. K. Meyer, and S. Zhang, *J. Mater. Chem. C* **3**, 339 (2015).
- [11] W. R. L. Lambrecht and A. Boonchun, *Phys. Rev. B* **87**, 195207 (2013).
- [12] J. S. Liu, C. X. Shan, H. Shen, B. H. Li, Z. Z. Zhang, L. Liu, L. G. Zhang, and D. Z. Shen, *Appl. Phys. Lett.* **101**, 011106 (2012).
- [13] J. G. Reynolds, C. L. Reynolds, A. Mohanta, J. F. Muth, J. E. Rowe, H. O. Everitt, and D. E. Aspnes, *Appl. Phys. Lett.* **102**, 152114 (2013).
- [14] S. Pal, T. Rakshit, S. S. Singha, K. Asokan, S. Dutta, D. Jana, and A. Sarkar, *J. Alloys Compd.* **703**, 26 (2017).
- [15] A. Chen, H. Zhu, Y. Wu, M. Chen, Y. Zhu, X. Gui, and Z. Tang, *Adv. Funct. Mater.* **26**, 3696 (2016).
- [16] M. Joseph, H. Tabata, and T. Kawai, *Jpn. J. Appl. Phys.* **38**, L1205 (1999).
- [17] Q. Peng, C. Liang, W. Ji, and S. De, *Comput. Mater. Sci.* **68**, 320 (2013).
- [18] H. Zheng, X.-B. Li, N.-K. Chen, S.-Y. Xie, W. Q. Tian, Y. Chen, H. Xia, S. B. Zhang, and H.-B. Sun, *Phys. Rev. B* **92**, 115307 (2015).
- [19] J. Lee, D. C. Sorescu, and X. Deng, *J. Phys. Chem. Lett.* **7**, 1335 (2016).
- [20] H.-K. Hong, J. Jo, D. Hwang, J. Lee, N. Y. Kim, S. Son, J. H. Kim, M.-J. Jin, Y. C. Jun, R. Erni, S. K. Kwak, J.-W. Yoo, and Z. Lee, *Nano Lett.* **17**, 120 (2017).
- [21] K. B. Tom, S. Lin, L. F. Wan, J. Wang, N. Ahlm, A. T. N'Diaye, K. Bustillo, J. Huang, Y. Liu, S. Lou, R. Chen, S. Yan, H. Wu, D. Jin, H. Yuan, D. Prendergast, and J. Yao, *ACS Nano* **12**, 7554 (2018).
- [22] T. Kumagai, S. Liu, A. Shiotari, D. Baugh, S. Shaikhutdinov, and M. Wolf, *J. Phys.: Condens. Matter* **28**, 494003 (2016).
- [23] H. M. Hill, A. F. Rigosi, C. Roquelet, A. Chernikov, T. C. Berkelbach, D. R. Reichman, M. S. Hybertsen, L. E. Brus, and T. F. Heinz, *Nano Lett.* **15**, 2992 (2015).
- [24] D. Wang, D. Han, X.-B. Li, S.-Y. Xie, N.-K. Chen, W. Q. Tian, D. West, H.-B. Sun, and S. B. Zhang, *Phys. Rev. Lett.* **114**, 196801 (2015).
- [25] D. Wang, D. Han, X.-B. Li, N.-K. Chen, D. West, V. Meunier, S. Zhang, and H.-B. Sun, *Phys. Rev. B* **96**, 155424 (2017).
- [26] P. Hohenberg and W. Kohn, *Phys. Rev.* **136**, B864 (1964).
- [27] W. Kohn and L. J. Sham, *Phys. Rev.* **140**, A1133 (1965).
- [28] G. Kresse and J. Furthmüller, *Comput. Mater. Sci.* **6**, 15 (1996).
- [29] G. Kresse and J. Furthmüller, *Phys. Rev. B* **54**, 11169 (1996).
- [30] J. P. Perdew, K. Burke, and M. Ernzerhof, *Phys. Rev. Lett.* **77**, 3865 (1996).
- [31] J. Heyd, G. E. Scuseria, and M. Ernzerhof, *J. Chem. Phys.* **118**, 8207 (2003).
- [32] J. Heyd, G. E. Scuseria, and M. Ernzerhof, *J. Chem. Phys.* **124**, 219906 (2006).
- [33] H. Karzel, W. Potzel, M. Köfferlein, W. Schiessl, M. Steiner, U. Hiller, G. M. Kalvius, D. W. Mitchell, T. P. Das, P. Blaha, K. Schwarz, and M. P. Pasternak, *Phys. Rev. B* **53**, 11425 (1996).
- [34] D. C. Reynolds, D. C. Look, B. Jogai, C. W. Litton, G. Cantwell, and W. C. Harsch, *Phys. Rev. B* **60**, 2340 (1999).
- [35] J. Tersoff and D. R. Hamann, *Phys. Rev. B* **31**, 805 (1985).
- [36] S. B. Zhang and J. E. Northrup, *Phys. Rev. Lett.* **67**, 2339 (1991).
- [37] D. Han, D. West, X.-B. Li, S.-Y. Xie, H.-B. Sun, and S. B. Zhang, *Phys. Rev. B* **82**, 155132 (2010).
- [38] D. Han, Y. Y. Sun, J. Bang, Y. Y. Zhang, H.-B. Sun, X.-B. Li, and S. B. Zhang, *Phys. Rev. B* **87**, 155206 (2013).
- [39] See Supplemental Material at <http://link.aps.org/supplemental/10.1103/PhysRevB.105.024104> for the additional data on computational method, atomic structures, density of states, molecular dynamics, and simulated STM images of monolayer ZnO.
- [40] B. Kaduk, T. Kowalczyk, and T. Van Voorhis, *Chem. Rev.* **112**, 321 (2012).
- [41] H. Q. Ta, L. Zhao, D. Pohl, J. Pang, B. Trzebicka, B. Rellinghaus, D. Pribat, T. Gemming, Z. Liu, A. Bachmatiuk, and M. H. Ruímmeli, *Crystals* **6**, 100 (2016).
- [42] C. Tusche, H. L. Meyerheim, and J. Kirschner, *Phys. Rev. Lett.* **99**, 026102 (2007).
- [43] C. H. Park, S. B. Zhang, and S.-H. Wei, *Phys. Rev. B* **66**, 073202 (2002).
- [44] M.-H. Du and S. B. Zhang, *Phys. Rev. B* **80**, 115217 (2009).
- [45] A. Carvalho, A. Alkauskas, A. Pasquarello, A. K. Tagantsev, and N. Setter, *Phys. Rev. B* **80**, 195205 (2009).
- [46] Y. Yan, M. M. Al-Jassim, and S.-H. Wei, *Appl. Phys. Lett.* **89**, 181912 (2006).
- [47] S. Masoumi, E. Nadimi, and F. Hossein-Babaei, *Phys. Chem. Chem. Phys.* **20**, 14688 (2018).
- [48] J. L. Lyons, A. Janotti, and C. G. Van de Walle, *Appl. Phys. Lett.* **95**, 252105 (2009).
- [49] S. B. Zhang, S. H. Wei, and A. Zunger, *Phys. Rev. B* **63**, 075205 (2001).
- [50] F. Oba, A. Togo, I. Tanaka, J. Paier, and G. Kresse, *Phys. Rev. B* **77**, 245202 (2008).
- [51] S. J. Clark, J. Robertson, S. Lany, and A. Zunger, *Phys. Rev. B* **81**, 115311 (2010).
- [52] S. Limpijumnong, S. B. Zhang, S.-H. Wei, and C. H. Park, *Phys. Rev. Lett.* **92**, 155504 (2004).
- [53] D. Wang, D. Han, D. West, N.-K. Chen, S.-Y. Xie, W. Q. Tian, V. Meunier, S. Zhang, and X.-B. Li, *npj Comput. Mater.* **5**, 8 (2019).
- [54] J. Ma, Z. G. Yu, and Y.-W. Zhang, *Phys. Rev. B* **95**, 165447 (2017).
- [55] H. Qiu, T. Xu, Z. Wang, W. Ren, H. Nan, Z. Ni, Q. Chen, S. Yuan, F. Miao, F. Song, G. Long, Y. Shi, L. Sun, J. Wang, and X. Wang, *Nat. Commun.* **4**, 2642 (2013).
- [56] D. Wang, X.-B. Li, and H.-B. Sun, *Nanoscale* **9**, 11619 (2017).
- [57] M. Li, J. Yao, X. Wu, S. Zhang, B. Xing, X. Niu, X. Yan, Y. Yu, Y. Liu, and Y. Wang, *ACS Appl. Mater. Interfaces* **12**, 6276 (2020).
- [58] J. Suh, T.-E. Park, D.-Y. Lin, D. Fu, J. Park, H. J. Jung, Y. Chen, C. Ko, C. Jang, Y. Sun, R. Sinclair, J. Chang, S. Tongay, and J. Wu, *Nano Lett.* **14**, 6976 (2014).
- [59] M. R. Laskar, D. N. Nath, L. Ma, E. W. Lee, C. H. Lee, T. Kent, Z. Yang, R. Mishra, M. A. Roldan, J.-C. Idrobo, S. T. Pantelides, S. J. Pennycook, R. C. Myers, Y. Wu, and S. Rajan, *Appl. Phys. Lett.* **104**, 092104 (2014).
- [60] H. Zheng, J. Kröger, and R. Berndt, *Phys. Rev. Lett.* **108**, 076801 (2012).
- [61] H. Zheng, A. Weismann, and R. Berndt, *Phys. Rev. Lett.* **110**, 226101 (2013).
- [62] K. Momma and F. Izumi, *J. Appl. Crystallogr.* **44**, 1272 (2011).